CMS Physics Analysis Summary

Contact: cms-pag-conveners-top@cern.ch 2016/07/14

Measurement of the differential production cross section for top-quark pairs as a function of jet multiplicity in the lepton+jets final state at $\sqrt{s} = 8$ TeV with the CMS detector

The CMS Collaboration

Abstract

The top-quark pair differential production cross section in pp collisions at $\sqrt{s} = 8$ TeV as a function of the number of jets is measured in the lepton+jets (e/μ+jets) final state for an integrated luminosity of 19.7 fb^{-1}. The cross section is presented in the visible phase space of the measurement as well as extrapolated to the full phase space. The results are compared with theoretical predictions at next-to-leading order. The comparisons show good agreement between the data and the predictions within the experimental and theoretical uncertainties.

1 Introduction

The associated production of top-quark pairs with additional jets ($t\bar{t}$+jets), which typically arise from initial- or final-state QCD radiation, is an important test of the validity and completeness of higher-order QCD calculations of processes leading to multijet events. Calculations at next-to-leading order (NLO) are available for $t\bar{t}$ pair production in association with one [1] or two [2] additional jets. Events from $t\bar{t}$+jets represent an important background to processes with multijet final states. One such process is the not yet observed associated production of a Higgs boson with a $t\bar{t}$ pair, with the Higgs boson decaying into a $b\bar{b}$ pair [3]. This process is one of the most promising channels for a direct measurement of the top quark Yukawa coupling. The correct description of $t\bar{t}$+jets production is also important in searches for new physics since several extensions of the standard model (SM) predict multijet final states.

The associated production of $t\bar{t}$+jets was studied by the ATLAS [4, 5] and CMS [6–9] collaborations at both $\sqrt{s} = 7$ and 8 TeV pp collisions. In this work, we present the measurement of the $t\bar{t}$ pair production cross section versus the jet multiplicity in two phase space definitions, visible and full. The visible phase space of the measurement is defined as the kinematic region in which all selected final-state objects are produced within the detector acceptance. The measurement in the visible phase space avoids additional model uncertainties arising from the extrapolation into the experimentally inaccessible regions of the full phase space. The results are corrected for detector effects and are compared at particle level with theoretical predictions obtained using different Monte Carlo (MC) event generators. The results are also normalized to the inclusive cross section measured *in situ*, in the same phase space, eliminating systematic uncertainties related to the normalization. Additionally, the cross section of the associated production of $t\bar{t}$+jets is extrapolated to the full phase space using correction factors obtained from simulation.

The results are based on the full 2012 data set of pp collisions at a center-of-mass energy of 8 TeV and corresponding to an integrated luminosity of 19.7 ± 0.5 fb^{-1}. The semileptonic decays of the $t\bar{t}$ pairs, where one of the W bosons decays into two quarks and the other to a charged lepton and a neutrino, are selected in the electron and muon channel. In these decays, the $t\bar{t}$ event is expected to have one lepton, missing transverse energy ($\not{E}_{\mathrm{T}}$) associated with the neutrino, and at least four jets associated to the $t\bar{t}$ system. The identification of jets originating from the fragmentation of b quarks in $t\bar{t}$ events is used to enhance the top quark signal over the background.

This document is organized as follows. In Section 2, the simulation of various physics processes is discussed. The reconstruction of physics objects and the event selection are discussed in Section 3. The background estimation methods are presented in Section 4. The measured quantities are defined in Section 5. The sources of systematic uncertainties and their effect on the results are described in Section 6. The results of the measurement are presented in Section 7, followed by a summary in Section 8.

2 Simulated samples

Simulated samples of the $t\bar{t}$+jets signal, and the background from W+jets, Z+jets and the associated $t\bar{t}$+V (W, Z) process are produced with the leading order (LO) matrix-element (ME) generator MADGRAPH (v5.1.5.11) [10], which implements the relevant matrix elements with up to three additional partons. The single top processes (s, t, and tW channels) are simulated with the NLO ME generator POWHEG (v1.0 r1380) [11–13]. The top-quark mass is fixed to M_{top}=172.5 GeV. Both generators are interfaced to PYTHIA (v6.426) [14] for the simulation of

parton shower (PS), hadronization and fragmentation. The same version of PYTHIA is used for simulations of the diboson (WW, WZ, and ZZ) and QCD multijet processes as well as the $t\bar{t}$+H process. The Higgs boson mass is set to M_H=125 GeV. The parton distribution function (PDF) set CTEQ6L1 [15] is used for the MADGRAPH and PYTHIA samples, while the CT10 [16] set is used for the POWHEG samples. For the underlying events the Z2* tune is employed [17]. A full detector simulation is performed with GEANT4 (v. 9.4) [18]. All produced samples are normalized to calculations of their corresponding inclusive cross sections [19–24]. The simulation includes the effect of additional pp collisions (pileup) [25] with a multiplicity matching the one observed in data.

The performance of all subdetectors is simulated in detail and validated with dedicated control samples. Possible residual differences between data and simulation in selection efficiencies of physics objects are accounted for by correction factors (described in Sections 3 and 6) calculated with various data-driven methods.

3 Physics object definition and event selection

Events are selected using single muon or single electron triggers that require $p_T^\mu > 24$ GeV, $|\eta^\mu| < 2.1$ and $p_T^e > 27$ GeV, $|\eta^e| < 2.5$ excluding a gap of $1.4442 < |\eta^e| < 1.5660$ between the barrel and endcap sections of the ECAL (ECAL gap). The leptons also satisfy isolation and track quality requirements.

The presence of at least one well reconstructed primary interaction vertex is required offline, with the longitudinal vertex position $|z_{PV}| < 24$ cm and with at least four tracks. In addition, the radial position (ρ) of the PV has to lie within the beam pipe: $|\rho_{PV}| < 2$ cm.

The reconstruction of the physics objects is based on the particle-flow (PF) algorithm that combines relevant information from all CMS subdetectors [26].

Electron candidates are reconstructed using hits in the tracker and energy deposits in the ECAL crystals [27]. Electrons should have a transverse momentum of $p_T^e > 30$ GeV and a pseudorapidity of $|\eta^e| < 2.5$ excluding the region of the ECAL gap. The electron should satisfy the PF quality criteria combined in a multivariate classifier (MVA) [28]. Electrons or positrons originating from photons decaying within the detector material are rejected by looking for conversion partners in the silicon tracker. The electron relative isolation I_{rel}^e is calculated as the sum of transverse energy of all charged and neutral particles measured in the tracker and calorimeters in a cone $\Delta R = \sqrt{\Delta\eta^2 + \Delta\phi^2} = 0.3$ around the electron divided by the electron transverse momentum p_T^e, where ϕ is the azimuthal angle. The value of the relative isolation should be $I_{\text{rel}}^e(\Delta R = 0.3) < 0.1$.

The muon momentum is reconstructed from hits in the tracker and matched segments in the muon chambers [29]. Muons should have $p_T^\mu > 30$ GeV, $|\eta^\mu| < 2.1$ and satisfy quality criteria related to the number of hits in the tracker, the muon track χ^2, the distance with respect to the primary interaction vertex [30] (PV), and the absolute distance in z between the PV and the muon track. Muons should be isolated. The relative isolation $I_{\text{rel}}^\mu(\Delta R = 0.4)$ is calculated in a similar way as for electrons but with a larger cone around the muon track. The relative isolation parameter should be $I_{\text{rel}}^\mu < 0.12$. Muons are reconstructed from a track in the tracking detector and in the muon system. The two tracks are then matched with a global fit and the normalized χ^2 per degree of freedom is required to be smaller than 10 in order to suppress hadronic punch-through and muons from decays in flight. Reduction of the fraction of misidentified muons is performed with additional requirements on the number of hits in the muon and tracker sub-

systems. Cosmic ray muons are rejected by restricting the position of the primary interaction vertex in the xy and z planes.

Events containing additional leptons defined with looser criteria are vetoed. Loose electrons have $p_{\mathrm{T}}^{e} > 20$ GeV, $I_{\mathrm{rel}}^{e} < 0.15$ and a MVA discriminator value greater than 0.5. Loose muons have $p_{\mathrm{T}}^{\mu} > 10$ GeV, $|\eta^{\mu}| < 2.5$ and looser requirements on track quality. Similarly to the loose electron, the loose muon is required to have a relaxed isolation criterion, namely, $I_{\mathrm{rel}}^{\mu} < 0.2$.

Jets are reconstructed with the anti-k_{T} algorithm [31] with a size parameter of $R = 0.5$. Jets should have $p_{\mathrm{T}}^{jet} > 30$ GeV and $|\eta^{jet}| < 2.5$ corresponding to the tracking-system acceptance. Each jet should have at least two constituents, charged or neutral, and should not be purely electromagnetic or hadronic. The charged hadron fraction in jets should be above zero. Jets are required to be separated from electrons or muons by $\Delta R(jet, [e, \mu]) > 0.5$. The energy scale of jets is corrected using a standard CMS procedure [32].

Jets from b quark hadronization are identified with the combined secondary vertex (CSV) algorithm that combines the use of secondary vertices together with different topological and kinematic variables such as the track impact parameter significance or the decay length of the B hadron inside the jet [33]. The working point used corresponds to a b tagging efficiency of about 70% and a mistag rate of about 1% and 15% for light-flavour (u, d, s and gluons) and c-quark jets, respectively. Correction factors are applied to the MC to account for small, residual differences between data and MC in the b tagging efficiency and mistag rate.

The event should contain exactly one lepton and at least four jets, with at least two of the jets identified as b jets. The presence of at least two b jets in the final state suppresses backgrounds which have a low probability to contain b jets. The presence of an isolated lepton together with b jets is very unlikely in QCD multijet or Z/γ^{*}+jets events, since the bottom quarks are mainly produced by the splitting of radiated gluons. Furthermore, the presence of at least four high-p_T jets reduces significantly backgrounds for which additional jets only appear through initial- or final- state radiation. The main background processes surviving the full selection are single top quark, W+jets and $\mathrm{t\bar{t}}+W/Z/H$ (significant only for high jet multiplicities).

4 Background determination

While the modeling of $\mathrm{t\bar{t}}+W/Z/H$, Z+jets, single top, and diboson background processes fully relies on the MC samples and dedicated cross-section calculations, the modeling of QCD multijet and W+jets background processes is achieved using data. This is necessary because of the poor modeling quality of jets misidentified as leptons achieved by the MC simulation of QCD multijet events and in order to improve the modeling of the jet flavour fractions produced in W+jets events, as motivated by [34]. No data-driven techniques are utilized for the Z+jets events since their expected yield is small.

Data are used to estimate the shape and normalization of the QCD multijet background and the normalization of the W+jets background in a data sample with no overlap with the signal region referred to as sideband region. The data-based background estimation is based on a binned maximum likelihood fit to data with selected events containing either two or three jets. The background estimation makes use of data and MC events containing exactly one b tagged jet (1-tag events) or at least two b tagged jets ($\geq$2-tags events), in order to enhance the discrimination between W+jets events that contain heavy-flavor (hf) jets from b and c quarks and W+jets events that contain light-flavor (lf) jets.

The QCD multijet model for each channel is extracted from data by replacing a tight require-

ment on the lepton by an inverted one. In the μ+jets channel, the relative isolation criterion is inverted, while the requirement that at least one lepton identification criterion has failed is applied in the e+jets channel. Contributions to the QCD multijet models originating from the $t\bar{t}$ signal and other non QCD multijet processes are subtracted according to the predictions of the MC simulation. For the W+jets background, the simulated sample is split into W+hf (containing jets matching bottom or charm quarks) and W+lf (all the rest) events.

A maximum likelihood fit is performed based on the $\not{E}_{\mathrm{T}}$ distribution, which provides good discrimination between QCD multijet events (no $\not{E}_{\mathrm{T}}$ expected) and the signal and W+jets events ($\not{E}_{\mathrm{T}}$ from the neutrino). The fit is performed simultaneously over four regions: e+jets or μ+jets events with 1-tag or $\geq$2-tags. For the QCD multijet model, the templates of the four regions are treated independently because different fit factors are expected in each region. Log-normal constraints corresponding to the uncertainties of the NLO predictions are applied to the Z+jets (3%) [21], $t\bar{t}$+$W/Z/H$ (10%) [23, 24] and diboson (5%) [22] background templates because of their small size and poor discrimination against other templates.

The results of the fit for W+hf, W+lf, and QCD multijet for e+jets and μ+jets events with $\geq$2-tags are then utilized in the signal region ($\geq$4 jets). The resulting normalization of the signal distribution is in agreement with the NNLO+NNLL prediction. The W+hf normalization is increased by almost a factor of 2 whereas the W+lf normalization is reduced to approximately 30% of the predicted value. This is compatible with the values utilized in [9].

The $t\bar{t}$+$W/Z/H$ background has negligible contribution at low jet multiplicity while at high jet multiplicity reaches 5% of selected events for both electron and muon channels. The non-$t\bar{t}$ backgrounds represent 12% (10%) of selected events for the final state with four or more jets in the electron (muon) channel and decrease to 4% (3%) as the jet multiplicity increases.

Distributions after applying the event selection are shown in Fig. 1, by combining the e+jets and μ+jets channels. The plots show the distributions of the number of selected jets (top left), the missing transverse energy (top right), the p_{T} and η of all selected jets (middle), and the p_{T} and η of the leading jet (bottom). The normalization of the QCD multijet and W+jets background processes is taken from the fit described above. The $t\bar{t}$ sample is scaled to the measured inclusive cross section described in Sec. 7.2.

5 Visible and Full Cross Sections

In this paper, two sets of measurements are presented. The first set corresponds to the measurement of the $t\bar{t}$ production cross section versus the particle-level jet multiplicity in the visible phase space. The second set corresponds to the measurement of the cross section of the associated production of $t\bar{t}$ with jets in the full phase space. The exact definitions of visible and full phase spaces are given in this section.

The "visible" cross section for i particle-level jets in the final state is defined as:

$$\frac{d\sigma_i}{dN_{\mathrm{jets}}} = \frac{\sum_j \mathrm{U}_{ij}(n_j^{\mathrm{data}} - n_j^{\mathrm{non\text{-}t\bar{t}}})}{\mathcal{L} \cdot \frac{(A\cdot\varepsilon)_i^{detec}}{(A\cdot\varepsilon)_i^{visible}}} \tag{1}$$

where $n_j^{data} - n_j^{non-t\bar{t}}$ represents the data yield for j reconstructed jets in the final state after the subtraction of the non-$t\bar{t}$ contributions, $\mathcal{L}$ is the integrated luminosity of the data set. The terms $(A\cdot\varepsilon)_i^{detec}$ and $(A\cdot\varepsilon)_i^{visible}$ are the product of acceptance times efficiency of events fulfilling the

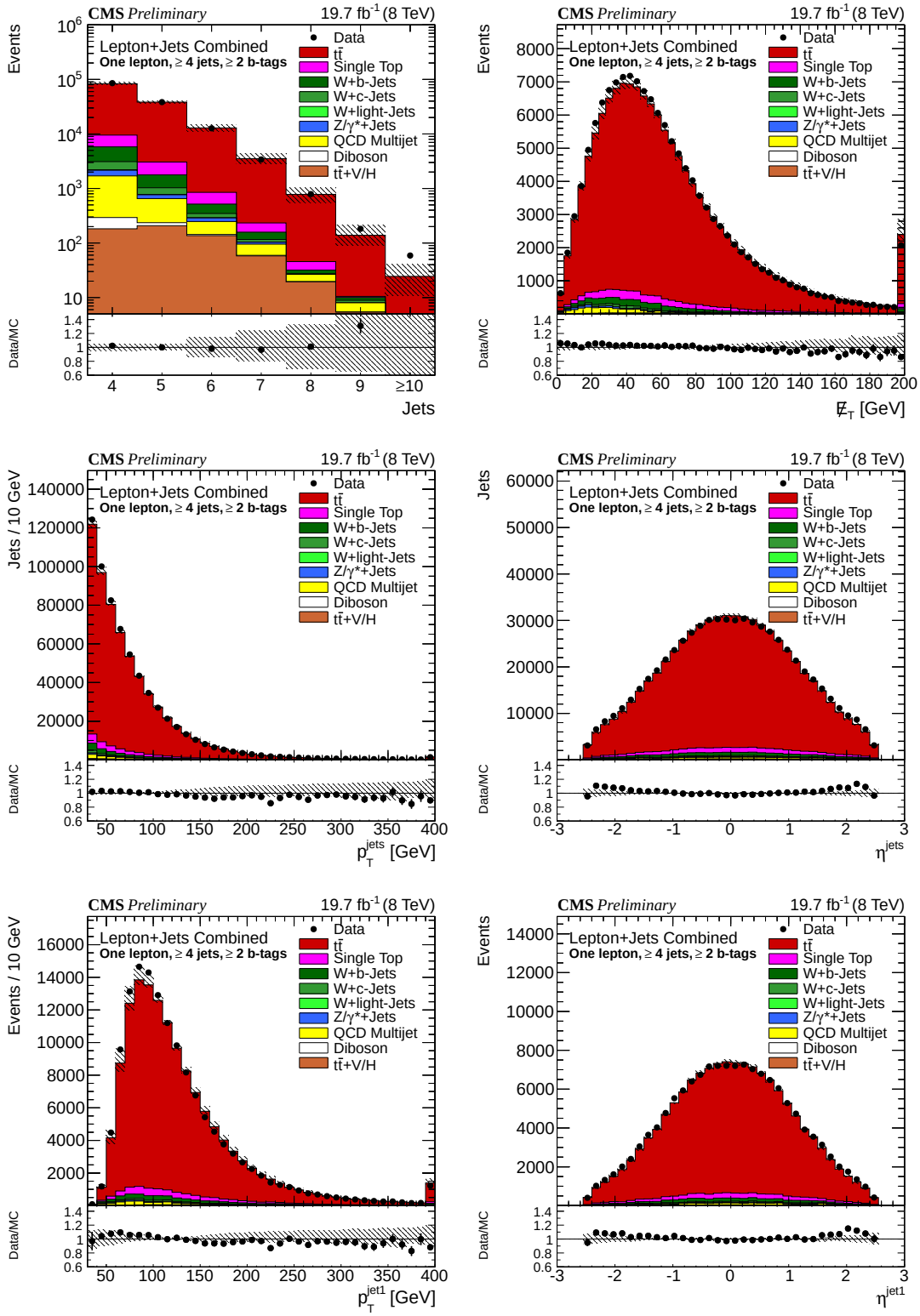

Figure 1: Distribution of the number of selected jets (top left), the missing transverse energy (top right), the p_{T} and η of all selected jets (middle), and the p_{T} and η of the leading jet (bottom), combining the e+jets and μ+jets channels. The lower part of each plot shows the ratio of the data to the MC predictions. The hashed areas represent the shape uncertainties affecting the MC signal and backgrounds. The normalization of the signal and background processes is discussed in the text.

detector-level and particle-level selection, respectively, for i particle-level jets.

The jet multiplicity yields are corrected for effects originating from the detection process by using a regularised unfolding procedure [9, 35, 36]. Based on the Singular Value Decomposition (SVD) method [37], the generalized inverse of the response matrix that connects the events with j reconstructed jets with the event with i particle-level jets is used to obtain the unfolded jet multiplicity distribution from the measured one. The elements of the inverse matrix are represented as U_{ij} in Eq. (1). A sum over the contributions from all reconstructed jet multiplicities is performed. The response matrix that accounts for event migrations is calculated from the simulated $t\bar{t}$ MADGRAPH (v5.1.5.11) sample. To avoid non-physical fluctuations arising from the matrix inversion, a smoothing prescription (regularisation) is applied [38]. The regularisation parameter for the SVD method is chosen in order to minimize the global correlation between neighbouring jet multiplicity bins of the unfolded distribution. The event migration in each bin is represented by the purity (number of events fulfilling the particle-level and the detector-level selection divided by the number of events fulfilling the detector-level selection) and the stability (same numerator as for the purity but divided by the number of events fulfilling the particle-level selection). The purity (stability) is at the level of 65% (80%) for the low jet multiplicity bins and drops to 30% (45%) for the high jet multiplicity bins for both e+jets and μ+jets channels.

The selection criteria for the definition of $(A \cdot \varepsilon)_i^{visible}$ for the visible phase space are defined as follows. For both the electron and muon final state, exactly one lepton at particle level is required with p_T >30 GeV and $|\eta| < 2.4$ while the particle-level jets should have p_T >30 GeV and $|\eta| < 2.5$. The presence of additional leptons with looser kinematic requirements ($p_{\mathrm{T}} > 15\,\mathrm{GeV}$ and $|\eta| < 2.5$) leads to the rejection of the event. Particle-level jets should have a distance of ΔR(jet, lepton)> 0.5 from the selected lepton.

The generated leptons at particle level are corrected for photon initial/final state radiation by clustering the photons and charged leptons around the lepton using the anti-k$_T$ algorithm with a distance parameter of $R = 0.1$.

The generated jets at particle level are clustered from all stable particles, except the clustered photons, charged leptons, and neutrinos, using the same algorithm as in real data. The b tagging of a jet at particle level is achieved by its association with one or more B hadrons with $p_{\mathrm{T}} > 5\,\mathrm{GeV}$. In order to include the B hadrons in the list of stable particles that will be used by the jet clustering algorithm, their energy is scaled to a negligible value, to cancel any bias on the nominal jet reconstruction [39]. The presence of a B hadron in the list of constituents of a resulting jet determines whether the jet is b tagged. Each event should have at least four particle-level jets and at least two of them have to be tagged as b jets.

Since the visible phase space measurement is defined purely with observable particles (at particle level), without utilizing any MC information defined before the parton showering and hadronization steps, its MC modeling dependence is negligible and hence it can be employed for model testing.

The full cross section for at least i additional particle-level jets in the final state is defined as:

$$\frac{d\sigma_{\geq i}}{dN_{\mathrm{jets}}} = \frac{(n_{\geq j}^{\mathrm{data}} - n_{\geq j}^{\mathrm{non\text{-}t\bar{t}}})}{\mathcal{L} \cdot \frac{(A\cdot\varepsilon)_{\geq j}^{detec}}{(A\cdot\varepsilon)_{\geq i}^{full}}} \ , \ \text{with } i = j - 4. \tag{2}$$

The term $n_{\geq j}^{data} - n_{\geq j}^{non-t\bar{t}}$ represents the data yield for at least j reconstructed jets in the final

state after the subtraction of the non-$t\bar{t}$ contributions, $\mathcal{L}$ is the integrated luminosity of the data set. The term $(A \cdot \varepsilon)^{detec}_{\geq j}$ is the product of acceptance times efficiency of events fulfilling the detector-level selection with at least j reconstructed jets in the final state and at least two of them being tagged as b jets and is estimated using MC events taking into account possible differences between data and simulation. The same detector-level selection is applied for both $n^{data}_{\geq j} - n^{non-t\bar{t}}_{\geq j}$ and $(A \cdot \varepsilon)^{detec}_{\geq j}$ terms.

The term $(A \cdot \varepsilon)^{full}_{\geq i}$ is the product of acceptance times efficiency of events fulfilling a predefined full phase space particle-level selection. The full phase space selection is common for electron or muon final states and requires $t\bar{t}$ events with at least i (i=0,1,2,3,4) additional particle-level jets with p_T >40 GeV, $|\eta|$ <2.5, and ΔR>0.5 between the additional jets. Additional jets are identified as those not matching any $t\bar{t}$ decay product geometrically (within ΔR=0.5). The i additional particle-level jets are connected to the j reconstructed jets via the relation $i = j$ - 4, where the four reconstructed jets correspond to the two b jets from the top quark decays and the hadronic decay of the W boson. There are no lepton selection criteria, since the $t\bar{t}$ pairs are considered as non-decayed. The result for $i = 2$ can be compared to the theoretical prediction [40] which is performed in the same full phase space.

6 Systematic Uncertainties

The yields, integrated luminosity, acceptance and efficiency terms of Eqs. (1-2) may be affected by different sources of systematic uncertainty. To estimate the effect of each source of uncertainty on the cross section measurement, the corresponding term is varied within its uncertainty and the resulting cross section is compared to the nominal one. The difference with respect to the nominal result is taken as the systematic uncertainty. The experimental uncertainties included are the uncertainties on the jet energy scale (JES) [32], the jet energy resolution (JER) [41], the scaling factors (SF) for lepton trigger and offline selection efficiencies, the b tagging efficiency scaling factors for different jets, the pileup reweighting and the integrated luminosity. Most theoretical uncertainties are related to the calculation of cross sections and the choice of different kinematic parameters in simulations. The majority of systematic uncertainties increase for higher jet multiplicities, unless stated otherwise.

The JES systematic uncertainty is estimated by shifting the energy scale of each reconstructed jet up and down by its uncertainty as a function of jet transverse momentum and pseudorapidity. This leads to 3.0-18.0% variation on the cross section measurement.

The jet energy resolution is observed to be degraded in data with respect to the simulated predictions. In order to correct for this effect, the jets in the MC simulation are smeared. Smearing uncertainties lead to a 0.1-4.5% variation on the cross section measurement.

The scale factors used to eliminate differences between data and simulation are varied within their uncertainties in order to estimate their effect on the trigger, lepton identification and isolation for both electrons and muons. This leads to a 0.4-0.8% variation on the cross section measurement, independent of jet multiplicity.

The uncertainties of the b tagging and mis-identification efficiency corrections applied to simulated samples are considered as sources of systematic uncertainties [33]. The correction factors are varied within their uncertainties resulting in a 0.1-4.4% variation on the cross section measurement. The size of the variation decreases as the jet multiplicity increases.

The uncertainty due to the modelling of pileup in the simulation is calculated by varying the

cross section assumed for inelastic pp collisions by $\pm 5\%$ from its central value. This leads to a 0.1-3.6% variation on the cross section measurement.

The uncertainty on the integrated luminosity is estimated to be 2.6% by an independent measurement [42]. It directly affects the cross section measurement as well as the normalization of simulated samples.

Uncertainties related to the unfolding procedure are taken into account resulting in a 1.3-31.3% variation on the cross section measurement.

Acceptance and efficiency corrections are derived using tree-level simulations produced with MADGRAPH+PYTHIA. The choice of renormalization and factorization scales introduces a systematic uncertainty which is estimated by varying the scales in the generation process. The calculation is performed using dedicated top pair and W+jets MC samples in which the scales are varied by shifting the MADGRAPH parameter Q, defined as Q^2=$M^2_{top,W}$+Σ $p^2_T(jet)$, by a factor of 2 and 0.5 for the upward and downward shift, respectively. This leads to a 0.2-18.0% variation on the cross section measurement.

The tree-level events produced by MADGRAPH are matched to the PYTHIA parton shower to model additional soft and collinear radiation. The thresholds that control the matching of partons from the matrix element with those from parton showers are varied in order to estimate the impact of the matching-threshold uncertainty on the measurement. The nominal jet-p_T threshold for the matching between the matrix-element jets and the parton showering jets for $t\bar{t}$ (W+jets) events is 20 (10) GeV. The threshold is varied by a factor of 2 and 0.5 which leads to a 1.0-40.3% variation on the cross section measurement.

A source of theoretical systematic uncertainties that can affect the cross section measurement is the PDF uncertainties. The PDF uncertainty calculation is performed using the "modified tolerance method" [43–45] with all eigenvector sets of the CT10 PDF. This leads to a 0.4-11.3% variation on the cross section measurement.

Results from POWHEG+PYTHIA which uses NLO matrix elements are obtained and compared to the default one (MADGRAPH+PYTHIA). The differences are treated as a systematic uncertainty that includes the differences in the order of matrix element calculations. This leads to a 0.2-25.2% variation on the cross section measurement.

The shape of the p_T spectrum of the individual top quarks in data [7] is found to be softer than predicted by various simulations at LO and NLO while the available approximate NNLO prediction delivers a reasonable description [46]. Based on these measurements, event SFs have been derived to estimate the potential impact of the modeling of the top quark p_T spectrum on the analysis. The systematic uncertainty is determined from the difference between applying and not applying the p_T reweighting. This leads to a 2.8-11.0% variation on the cross section measurement.

The data-driven estimation of the QCD multijet and W+jets backgrounds leads to cross section uncertainties from the template fit. The resulting uncertainties are increased in order to cover correlations across electron and muon channels. Moreover, uncertainties on the shape of the background models used in the fit are taken into account. Background uncertainties lead to a 0.1-3.3% variation on the cross section measurement.

Table 1: Production cross section of $t\bar{t}$ pairs versus the particle-level jet multiplicity in the ℓ+jets channel. The relative statistical, experimental, theoretical and total uncertainties are also shown. Total uncertainties include the luminosity uncertainty of 2.6%.

Category	$d\sigma/dN_{jets}$ [pb]	Stat.	Exp.	Theor.	Total
$t\bar{t} \to \ell$ + 4 jets	4.15	1.0%	6.2%	5.3%	8.6%
$t\bar{t} \to \ell$ + 5 jets	1.88	1.3%	7.4%	7.0%	10.6%
$t\bar{t} \to \ell$ + 6 jets	0.615	2.6%	8.7%	8.5%	12.7%
$t\bar{t} \to \ell$ + 7 jets	0.156	5.9%	13.6%	11.7%	19.1%
$t\bar{t} \to \ell$ + 8 jets	0.0352	13.4%	19.1%	19.3%	30.4%
$t\bar{t} \to \ell$ + 9 jets	0.0116	16.7%	24.3%	33.3%	44.6%
$t\bar{t} \to \ell + \geq 10$ jets	0.00413	18.7%	27.9%	34.6%	48.3%

Table 2: Normalized production cross section of $t\bar{t}$ pairs versus the particle-level jet multiplicity in the ℓ+jets channel. The relative statistical, experimental, theoretical and total uncertainties are also shown.

Category	$1/\sigma\ d\sigma/dN_{jets}$	Stat.	Exp.	Theor.	Total
$t\bar{t} \to \ell$ + 4 jets	0.605	0.4%	1.7%	1.8%	2.5%
$t\bar{t} \to \ell$ + 5 jets	0.275	0.7%	2.2%	2.6%	3.4%
$t\bar{t} \to \ell$ + 6 jets	0.0897	2.9%	4.4%	4.2%	6.7%
$t\bar{t} \to \ell$ + 7 jets	0.0228	5.4%	9.2%	7.9%	13.3%
$t\bar{t} \to \ell$ + 8 jets	0.00514	13.2%	16.3%	16.8%	26.9%
$t\bar{t} \to \ell$ + 9 jets	0.00170	15.1%	21.0%	28.8%	38.7%
$t\bar{t} \to \ell + \geq 10$ jets	0.000603	17.1%	24.6%	30.8%	43.0%

7 Results

The $t\bar{t}$ pair production cross section is measured using the electron and muon final states. The ratio of the cross sections in the two channels for each jet multiplicity is consistent with 1.0 within uncertainties so the results of the two channels are combined using the best linear unbiased estimator (BLUE) method [47–49]. Correlations of the systematic uncertainties between the different channels and jet multiplicity bins are taken into account. For the combination of the cross section measurements it is assumed that the theoretical uncertainties and the experimental uncertainties related to jets and b tagging are fully correlated between electron and muon channels. All other experimental uncertainties are considered as uncorrelated.

7.1 Cross section versus the particle-level jet multiplicity in the visible phase space

The $t\bar{t}$ pair production cross section versus the particle-level jet multiplicity is measured in the visible phase space. The total uncertainties are dominated by systematic uncertainties over the entire jet multiplicity range. The combined results are shown in Table 1. The results are also normalized to the inclusive cross section measured *in situ*, in the same phase space, eliminating systematic uncertainties related to the normalization. The normalized combined results are shown in Table 2.

The experimental results are compared to predictions from MC samples produced with the nominal MADGRAPH+PYTHIA simulation at leading order (LO), and from alternative generators including the next-to-leading order (NLO) generators POWHEG+PYTHIA, POWHEG+HERWIG (v6.520 [50]), and MC@NLO(v3.40 [51])+HERWIG. A comparison between the measured cross section and the predictions is presented in Fig. 2 (top). This first comparison shows good

agreement between data and the nominal MADGRAPH+PYTHIA predictions for events with 4 to 7 jets. This can be explained by the explicit requirement of 0 to 3 additional jets at matrix-element level per $t\bar{t}$ pair, which exactly correspond to 4 to 7 jets when all decay products of the $t\bar{t}$ pair have produced well measured jets in the ℓ+jets channel. Even better agreement is observed between the results and predictions from NLO generators POWHEG+PYTHIA and POWHEG+HERWIG. However, the NLO prediction from MC@NLO+HERWIG provides a lower jet multiplicity. For 6 jets and more, the prediction from MC@NLO+HERWIG is more than two standard deviations below the measurement. At the highest jet multiplicities, too few events are predicted by all generators, where POWHEG+HERWIG shows the smallest disagreement.

The results are also compared (Fig. 2 bottom) to predictions from MADGRAPH+PYTHIA generators with varied parameters for the factorization and renormalization scale. The variation of the matching threshold has a significant impact on the MADGRAPH+PYTHIA predictions in events with at least 8 jets, but the variation of the Q^2 scale has a larger effect starting from events with 5 jets. For both parameters a modification of the shape of the predicted jet-multiplicity spectrum is observed. Increasing the matching threshold improves the agreement with the measurement at high jet multiplicity ($\geq$8 jets). Decreasing the matching threshold makes the agreement with data worse than MADGRAPH+PYTHIA at high jet multiplicity ($\geq$8 jets). Increasing the Q^2 scale reduces the probability of additional radiation. Hence the predicted spectrum is shifted to lower jet multiplicities: the prediction disagrees with the measurement for events with at least 5 jets. As expected, decreasing the Q^2 scale shows the opposite effect for events with 4 to 7 jets, causing more additional emissions. Nevertheless, the trend is reversed for $\geq$8 jets, where the additional-jet production is too weak, so the impact of decreasing the Q^2 scale does not affect the radiation of more additional observable jets anymore. The difference between the MADGRAPH+PYTHIA predicted jet-multiplicity spectrum with $4 \times Q^2$ and $Q^2/4$ scale variation is significantly larger than the measurement uncertainties.

The particle-level selection has been implemented in a modern tool for model validation, the Robust Independent Validation of Experiment and Theory (RIVET v1.8.2) [52]. It enables the calculation of the differential visible cross section predictions from various MC generators, thus providing further comparisons with measurements. The RIVET framework is designed to be robust by allowing only the final state particles in the HepMC [53] data format. This ensures independence from unphysical information in the generators and direct theory versus data comparisons. In Fig. 3 we present a comparison with predictions from aMC@NLO [54] and SHERPA v2.1.1 [55]. The aMC@NLO generator has been configured to produce $t\bar{t}$ events with zero, one, and two additional emissions at NLO. It is interfaced with PYTHIA8 [14, 56] for the parton-showering and hadronization. Two configurations are tested with SHERPA. In the first configuration, $t\bar{t}$+0 additional jets is simulated at NLO, while in the second $t\bar{t}$+0 and $t\bar{t}$+1 additional jets are simulated at NLO and merged. In both cases, further emissions, up to three, are simulated with LO precision. Samples of $t\bar{t}$ events generated with these configurations have been analyzed and compared to the unfolded data presented in the previous section. The sensitivity of the MC simulation to Q^2 scale variation is investigated through the variation of its nominal value with factors of 4 and 1/4.

The predictions from aMC@NLO are in marginal agreement with the measured differential production cross section. Slightly too high predictions are seen for 6 and 7 jets, but at the highest jet multiplicity the performance is still competitive against e.g. MADGRAPH. The predictions from SHERPA for $t\bar{t}$+0 additional parton emission at NLO show a good description of the jet-multiplicity spectrum, up to 8 jets, comparable to the MADGRAPH predictions. Predictions from SHERPA for $t\bar{t}$+0 and 1 additional parton emission at NLO are in agreement with the differential production cross section measurement except for 7 jets, where the prediction

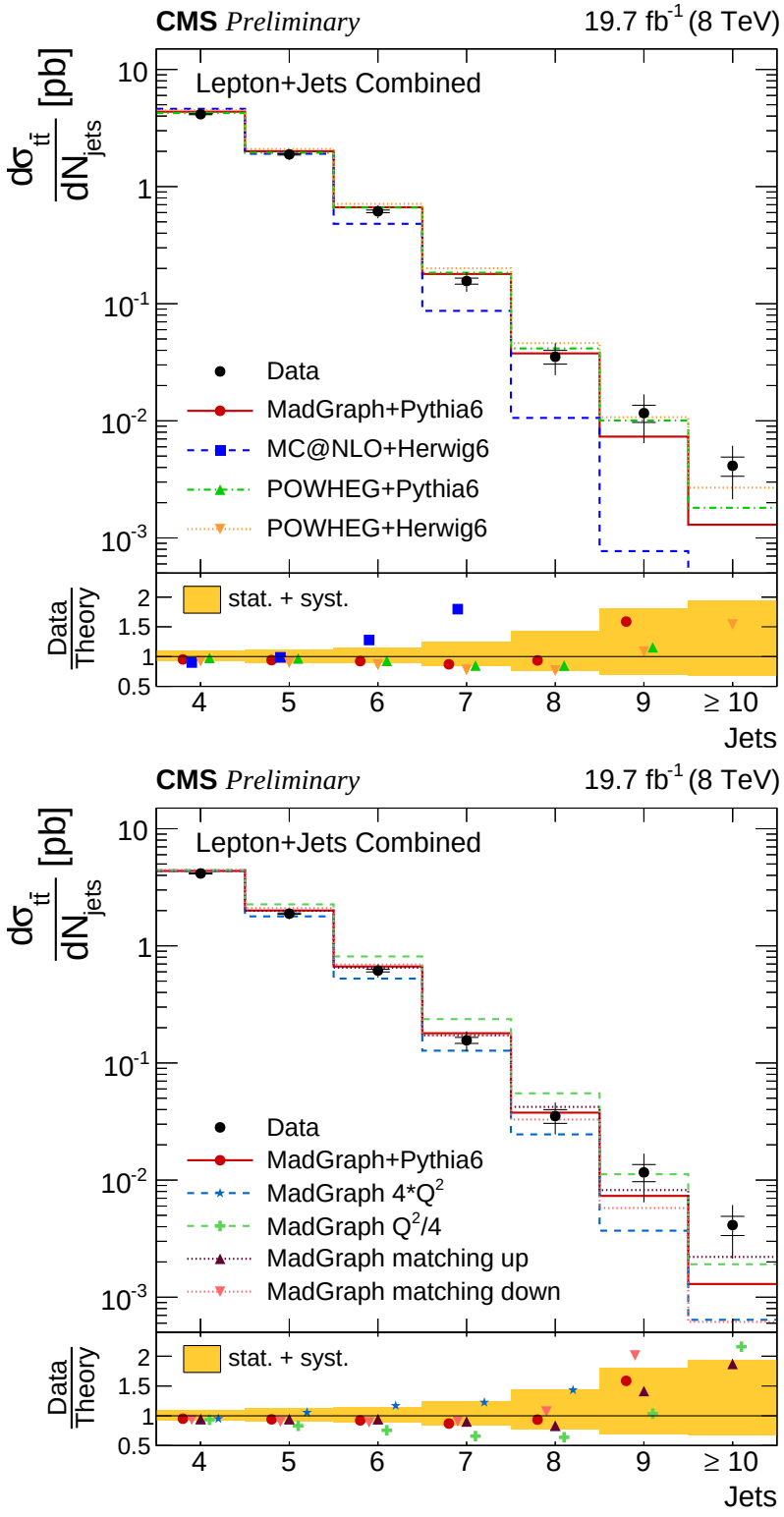

Figure 2: Combined differential visible $t\bar{t}$ cross section as a function of the number of particle-level jets in the ℓ+jets channel. The results are compared to predictions from various generators (top) or from MADGRAPH with various parameter sets (bottom). The vertical bars represent the total uncertainties and the intersecting horizontal bars represent the statistical uncertainties alone. In the ratio plot for MC@NLO and MADGRAPH with varied Q^2 value, the band represents the uncertainty of the measurement.

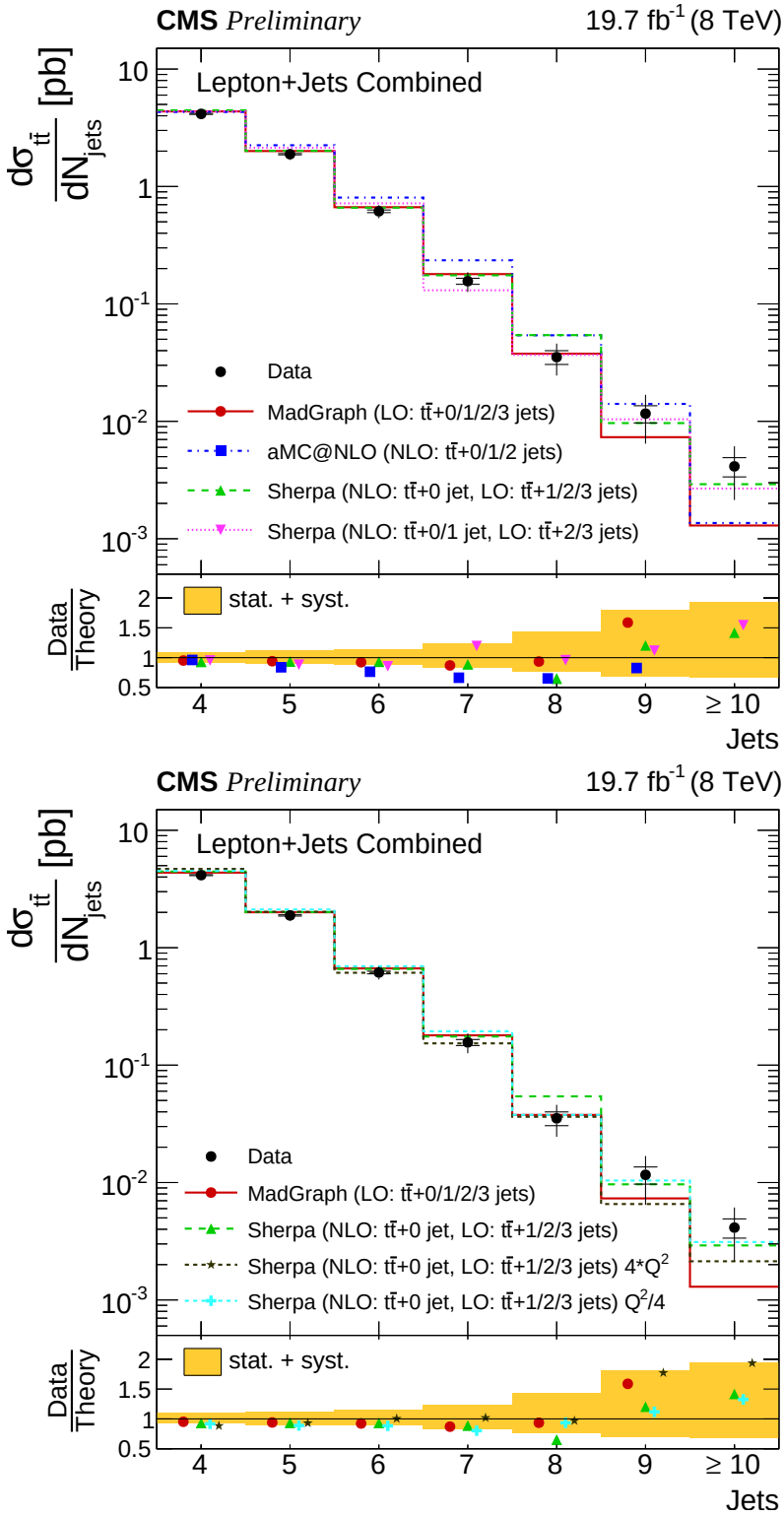

Figure 3: Combined differential visible $\mathrm{t\bar{t}}$ cross section as a function of the number of particle-level jets in the ℓ+jets channel. The results are compared to predictions from various MC generators (top) and SHERPA Q^2 (bottom). The vertical bars represent the total uncertainties and the intersecting vertical bars represent the statistical uncertainties alone. In the ratio plot, the band represents the uncertainty of the measurement.

Table 3: Comparison between the measured differential production cross section and predictions from various generators. A χ^2 and a p-value are calculated using the covariance matrix of the measured cross sections. The number of degrees of freedom (NDF) are equal to the number of the jet multiplicity bins.

generators	χ^2/NDF	p-value
MADGRAPH+PYTHIA6	4.9/7	0.7
MC@NLO+HERWIG6	34.7/7	<0.01
POWHEG+PYTHIA6	3.9/7	0.8
POWHEG+HERWIG6	4.4/7	0.7
aMC@NLO (NLO: $t\bar{t}$+0/1/2 jets)	20.0/7	<0.01
SHERPA (NLO: $t\bar{t}$+0 jet, LO: $t\bar{t}$+1/2/3 jets)	4.3/7	0.7
SHERPA (NLO: $t\bar{t}$+0/1 jet, LO: $t\bar{t}$+2/3 jets)	11.3/7	0.13

is significantly lower than data. In Fig. 3 (bottom), the effect of the Q^2-scale uncertainties is tested on SHERPA simulation of $t\bar{t}$+0 emissions at NLO. In comparison with predictions from MADGRAPH, the sensitivity to Q^2 scale variation is smaller, as can be seen when comparing with Fig. 2. This is mostly visible for 6 and 7 jets: predictions from SHERPA with Q^2 scale varied up or down are still contained within the measurement uncertainties, which is not the case for the MADGRAPH predictions. This confirms that, as expected, using NLO calculations reduces the sensitivity to Q^2-scale uncertainties, compared to LO.

The level of agreement between the measured differential production cross section and predictions from various generators is quantified by calculating χ^2 values, employing the full covariance matrices and inferring p-values from the χ^2 and the number of degrees of freedom (NDF). The results of calculations are collected in Table 3.

7.2 Cross section of the associated production of $t\bar{t}$ pairs with jets in the full phase space

The cross section of the associated production of $t\bar{t}$ pairs with jets is extrapolated to the full phase space in the electron and muon final states. The results from the combination of the electron and muon channels, together with available theory predictions, are shown in Table 4.

Table 4: Associated production cross section of $t\bar{t}$ pairs with 0–4 jets in the final state, from the combination of the e+jets and μ+jets channels, extrapolated to the full phase space. The relative statistical, experimental, theoretical and total uncertainties are also shown. Total uncertainties include the luminosity uncertainty of 2.6%.

	$d\sigma/dN$ [pb]	Stat.	Exp.	Theo.	Total	Prediction [pb]
$t\bar{t} + \geq 0$ jet	239.9	0.3%	6.2%	11.2%	13.0%	$252.9^{+2.5\%}_{-3.4\%}(\text{scale}) \pm 4.6\%(\text{PDF}+\alpha_s)$
$t\bar{t} + \geq 1$ jet	81.4	0.5%	7.2%	11.7%	14.0%	-
$t\bar{t} + \geq 2$ jets	20.1	0.8%	8.5%	13.6%	16.3%	$20.97^{-15.5\%}_{-13.3\%}(\text{scale})$
$t\bar{t} + \geq 3$ jets	4.06	1.6%	10.3%	18.4%	21.3%	-
$t\bar{t} + \geq 4$ jets	0.71	3.4%	13.1%	30.5%	33.4%	-

The measured cross section for $t\bar{t} + \geq 0$ jet

$$\sigma^{\text{meas}}_{t\bar{t}} = 239.9 \pm 0.7(\text{stat.}) \pm 14.8(\text{exp.}) \pm 26.8(\text{theo.}) \pm 6.2(\text{lum.}) \text{ pb}, \quad (3)$$

corresponds to the full $t\bar{t}$ cross section. The sources of the experimental and theoretical uncer-

tainties taken into account are described in Section 6. The measured cross section is in good agreement with the latest prediction:

$$\sigma_{t\bar{t}}^{\text{pred}} = 252.9^{+6.4}_{-8.6}(\text{scale}) \pm 11.7(\text{PDF} + \alpha_s) \text{ pb}, \quad (4)$$

as calculated with the Top++2.0 program to next-to-next-to-leading order in perturbative QCD, including soft-gluon resummation to next-to-next-to-leading-log order (see [19] and references therein), and assuming a top-quark mass of $m_t = 172.5\,\text{GeV}$. The first uncertainty arises from the independent variation of the factorization and renormalization scales, while the second one is associated to variations in the PDF and α_s, following the PDF4LHC prescription with the MSTW2008 68% CL NNLO, CT10 NNLO and NNPDF2.3 5f FFN PDF sets (see [57] and references therein, and [58–60]). The result is also in agreement with the published measurement from the CMS experiment [6] at $\sqrt{s} = 8$ TeV.

Moreover, the results of the measurement of $t\bar{t} + \geq 2$ jets

$$\sigma_{t\bar{t}+\geq 2\text{jets}}^{\text{meas}} = 20.1 \pm 0.2(\text{stat.}) \pm 1.7(\text{exp.}) \pm 2.7(\text{theo.}) \pm 0.5(\text{lum.}) \text{ pb}, \quad (5)$$

can be compared to predictions in [40]:

$$\sigma_{t\bar{t}+\geq 2\text{jets}}^{\text{pred}} = 20.97^{-3.25}_{-2.79}\,\text{pb}, \quad (6)$$

where the uncertainties originate from the scale uncertainty only. One should note that this calculation is performed assuming a top-quark mass of $m_t = 173.5\,\text{GeV}$, hence different from m_t assumed for the measurement. The measurement of $t\bar{t} + \geq 2$ jets cross section was also performed in the context of another CMS analysis at $\sqrt{s} = 8$ TeV [8]. The CMS analysis in the dilepton channel reported an absolute cross section of $\sigma_{t\bar{t}+\geq 2\text{jets}} = 16.1 \pm 0.7(\text{stat}) \pm 2.1(\text{syst} \oplus \text{lumi})$ pb in agreement within uncertainties with the measurement reported in this work.

8 Summary

The differential production cross section of a top-quark pair as a function of the number of jets is presented in the lepton+jet final state for an integrated luminosity of 19.7 fb^{-1} at $\sqrt{s} = 8$ TeV pp collisions. The cross section is presented in the visible phase space of the measurement for exactly 4–9 and 10 or more particle-level jets in the final state as well as to the extrapolated full phase space for equal or more than 0–4 additional jets. The results are compared with the theoretical predictions as well as other published experimental results. The comparisons show consistency with the predictions within the experimental and theoretical uncertainties. The measurement in the visible phase space have been performed in a way to be fully compatible with predictions at particle level for model testing purposes.

References

[1] S. Dittmaier, P. Uwer, and S. Weinzierl, "NLO QCD corrections to t anti-t + jet production at hadron colliders", *Phys. Rev. Lett.* **98** (2007) 262002, doi:10.1103/PhysRevLett.98.262002, arXiv:hep-ph/0703120.

[2] G. Bevilacqua, M. Czakon, C. Papadopoulos, and M. Worek, "Hadronic top-quark pair production in association with two jets at Next-to-Leading Order QCD", *Phys. Rev. D* **84** (2011) 11401, arXiv:1108.2851.

[3] CMS Collaboration, "Search for the standard model Higgs boson produced in association with a top-quark pair in pp collisions at the LHC", *JHEP* **05** (2013) 145, doi:10.1007/JHEP05(2013)145, arXiv:1303.0763.

[4] ATLAS Collaboration, "Measurement of the $t\bar{t}$ production cross-section as a function of jet multiplicity and jet transverse momentum in 7 TeV proton-proton collisions with the ATLAS detector", *JHEP* **01** (2015) 020, doi:10.1007/JHEP01(2015)020, arXiv:1407.0891.

[5] ATLAS Collaboration, "Measurements of fiducial cross-sections for $t\bar{t}$ production with one or two additional b-jets in pp collisions at $\sqrt{s}$ =8 TeV using the ATLAS detector", *Eur. Phys. J.* **C76** (2016), no. 1, 11, doi:10.1140/epjc/s10052-015-3852-4, arXiv:1508.06868.

[6] CMS Collaboration, "Measurement of the $t\bar{t}$ production cross section in the dilepton channel in pp collisions at $\sqrt{s}$ = 8 TeV", *JHEP* **02** (2014) 024, doi:10.1007/JHEP02(2014)024, 10.1007/JHEP02(2014)102, arXiv:1312.7582. [Erratum: JHEP02,102(2014)].

[7] CMS Collaboration, "Measurement of the differential cross section for top quark pair production in pp collisions at $\sqrt{s} = 8$ TeV", *Eur. Phys. J.* **C75** (2015), no. 11, 542, doi:10.1140/epjc/s10052-015-3709-x, arXiv:1505.04480.

[8] CMS Collaboration, "Measurement of the cross section ratio $\sigma_{t\bar{t}b\bar{b}}/\sigma_{t\bar{t}jj}$ in pp collisions at $\sqrt{s}$ = 8 TeV", *Phys. Lett.* **B746** (2015) 132–153, doi:10.1016/j.physletb.2015.04.060, arXiv:1411.5621.

[9] CMS Collaboration, "Measurement of jet multiplicity distributions in $t\bar{t}$ production in pp collisions at $\sqrt{s} = 7$ TeV", *Eur. Phys. J.* **C74** (2015) 3014, doi:10.1140/epjc/s10052-014-3014-0, 10.1140/epjc/s10052-015-3437-2, arXiv:1404.3171. [Erratum: Eur. Phys. J.C75,no.5,216(2015)].

[10] J. Alwall et al., "MADGRAPH 5 : Going Beyond", *JHEP* **06** (2011) 128, arXiv:1106.0522.

[11] P. Nason, "A New method for combining NLO QCD with shower Monte Carlo algorithms", *JHEP* **0411** (2004) 040, doi:10.1088/1126-6708/2004/11/040, arXiv:hep-ph/0409146.

[12] S. Frixione, P. Nason, and C. Oleari, "Matching NLO QCD computations with Parton Shower simulations: the POWHEG method", *JHEP* **11** (2007) 070, doi:10.1088/1126-6708/2007/11/070, arXiv:0709.2092.

[13] S. Alioli, P. Nason, C. Oleari, and M. Re, "A general framework for implementing NLO calculations in shower Monte Carlo programs: the POWHEG BOX", *JHEP* **1006** (2010) 043, doi:10.1007/JHEP06(2010)043, arXiv:1002.2581.

[14] T. Sjöstrand, S. Mrenna, and P. Z. Skands, "PYTHIA 6.4 physics and manual", *JHEP* **05** (2006) 026, arXiv:hep-ph/0603175.

[15] J. Pumplin et al., "New generation of parton distributions with uncertainties from global QCD analysis", *JHEP* **07** (2002) 012, doi:10.1088/1126-6708/2002/07/012, arXiv:hep-ph/0201195.

[16] H.-L. Lai et al., "New parton distributions for collider physics", *Phys. Rev.* **D82** (2010) 074024, doi:10.1103/PhysRevD.82.074024, arXiv:1007.2241.

[17] R. Field, "Min-bias and the underlying event at the LHC", *Acta Physics Polonica B* **42** (2011) 2631.

[18] GEANT4 Collaboration, "GEANT4 – a simulation toolkit", *Nucl. Instrum. Meth. A* **506** (2003) 250.

[19] M. Czakon and A. Mitov, "Top++: A Program for the Calculation of the Top-Pair Cross-Section at Hadron Colliders", *Comput. Phys. Commun.* **185** (2014) 2930, doi:10.1016/j.cpc.2014.06.021, arXiv:1112.5675.

[20] N. Kidonakis, "Differential and total cross sections for top pair and single top production", doi:10.3204/DESY-PROC-2012-02/251, arXiv:1205.3453.

[21] K. Melnikov and F. Petriello, "Electroweak gauge boson production at hadron colliders through O(alpha(s)**2)", *Phys.Rev.* **D74** (2006) 114017, doi:10.1103/PhysRevD.74.114017, arXiv:hep-ph/0609070.

[22] J. M. Campbell and R. K. Ellis, "Radiative corrections to Z b anti-b production", *Phys.Rev.* **D62** (2000) 114012, doi:10.1103/PhysRevD.62.114012, arXiv:hep-ph/0006304.

[23] J. M. Campbell and R. K. Ellis, "$t\bar{t}W^{+-}$ production and decay at NLO", *JHEP* **07** (2012) 052, doi:10.1007/JHEP07(2012)052, arXiv:1204.5678.

[24] M. V. Garzelli, A. Kardos, C. G. Papadopoulos, and Z. Trocsanyi, "t $\bar{t}$ W^{+-} and t $\bar{t}$ Z Hadroproduction at NLO accuracy in QCD with Parton Shower and Hadronization effects", *JHEP* **11** (2012) 056, doi:10.1007/JHEP11(2012)056, arXiv:1208.2665.

[25] G. Antchev et al., "First measurement of the total proton-proton cross section at the LHC energy of $\sqrt{s}$ =7 TeV", *Europhys. Lett.* **96** (2011) 21002, doi:10.1209/0295-5075/96/21002, arXiv:1110.1395.

[26] CMS Collaboration, "Commissioning of the Particle-Flow reconstruction in Minimum-Bias and Jet Events from pp Collisions at 7 TeV", CMS Physics Analysis Summary CMS-PAS-PFT-10-002, CERN, Geneva, 2010.

[27] CMS Collaboration, "Performance of electron reconstruction and selection with the CMS detector in proton-proton collisions at $\sqrt{s} = 8$ TeV", *JINST* **10** (2015), no. 06, P06005, doi:10.1088/1748-0221/10/06/P06005, arXiv:1502.02701.

[28] A. Hoecker et al., "TMVA - Toolkit for Multivariate Data Analysis", *PoS ACAT* **040** (2007) arXiv:0703039.

[29] CMS Collaboration, "Performance of CMS muon reconstruction in pp collision events at $\sqrt{s} = 7$ TeV", *JINST* **7** (2012) P10002, arXiv:1206.4071.

[30] CMS Collaboration, "Description and performance of track and primary-vertex reconstruction with the CMS tracker", *JINST* **9** (2014), no. 10, P10009, doi:10.1088/1748-0221/9/10/P10009, arXiv:1405.6569.

[31] M. Cacciari, G. Salam, and G. Soyez, "The anti-kt jet clustering algortihm", *JHEP* **04** (2008) 063, arXiv:0802.1189.

[32] CMS Collaboration, "Determination of Jet Energy Calibration and Transverse Momentum Resolution in CMS", *JINST* **6** (2011) P11002, doi:10.1088/1748-0221/6/11/P11002, arXiv:1107.4277.

[33] CMS Collaboration, "Identification of b-quark jets with the CMS experiment", *JINST* **8** (2013) P04013, doi:10.1088/1748-0221/8/04/P04013, arXiv:1211.4462.

[34] CMS Collaboration, "Measurement of the $t\bar{t}$ production cross section in pp collisions at $\sqrt{s} = 7$ TeV with lepton + jets final states", *Physics Letters B* **720** (2013), no. 120133, 83 – 104, doi:10.1016/j.physletb.2013.02.021. http://www.sciencedirect.com/science/article/pii/S0370269313001500.

[35] V. Blobel, "An Unfolding method for high-energy physics experiments", in *Advanced statistical techniques in particle physics. Proceedings, Conference, Durham, UK, March 18-22, 2002*, pp. 258–267. 2002. arXiv:hep-ex/0208022.

[36] CMS Collaboration, "Inclusive and differential measurements of the $t\bar{t}$ charge asymmetry in pp collisions at $\sqrt{s} = 8$ TeV", arXiv:1507.03119.

[37] A. Höcker and V. Kartvelishvili, "SVD approach to data unfolding", *Nucl. Instrum. Meth.* **A372** (1996) 469–481, doi:10.1016/0168-9002(95)01478-0, arXiv:hep-ph/9509307.

[38] F. James, "Statistical Methods in Experimental Physics". World Scientific, Singapore, 2 edition, 2006.

[39] M. Cacciari, G. P. Salam, and G. Soyez, "The Catchment Area of Jets", *JHEP* **04** (2008) 005, doi:10.1088/1126-6708/2008/04/005, arXiv:0802.1188.

[40] G. Bevilacqua and M. Worek, "On the ratio of $t\bar{t}b\bar{b}$ and $t\bar{t}jj$ cross sections at the CERN Large Hadron Collider", *JHEP* **07** (2014) 135, doi:10.1007/JHEP07(2014)135, arXiv:1403.2046.

[41] CMS Collaboration, "Jet Energy Resolution in CMS at $\sqrt{s} = 7$ TeV", CMS Physics Analysis Summary CMS-PAS-JME-10-014, CERN, Geneva, 2011.

[42] CMS Collaboration, "CMS Luminosity Based on Pixel Cluster Counting - Summer 2013 Update", CMS Physics Analysis Summary CMS-PAS-LUM-13-001, CERN, Geneva, 2013.

[43] D. Bourilkov, R. C. Group, and M. R. Whalley, "LHAPDF: PDF use from the Tevatron to the LHC", in *TeV4LHC Workshop - 4th meeting Batavia, Illinois, October 20-22, 2005*. 2006. arXiv:hep-ph/0605240.

[44] Z. Sullivan and P. M. Nadolsky, "Heavy quark parton distribution functions and their uncertainties", *eConf* **C010630** (2001) P511, arXiv:hep-ph/0111358.

[45] P. M. Nadolsky and Z. Sullivan, "PDF uncertainties in WH production at Tevatron", *eConf* **C010630** (2001) P510, arXiv:hep-ph/0110378.

[46] N. Kidonakis, "NNLL threshold resummation for top-pair and single-top production", *Phys. Part. Nucl.* **45** (2014), no. 4, 714–722, doi:10.1134/S1063779614040091, arXiv:1210.7813.

[47] L. Lyons, D. Gibaut, and P. Clifford, "How to Combine Correlated Estimates of a Single Physical Quantity", *Nucl. Instrum. Meth.* **A270** (1988) 110, doi:10.1016/0168-9002(88)90018-6.

[48] A. Valassi, "Combining correlated measurements of several different physical quantities", *Nucl. Instrum. Meth.* **A500** (2003) 391–405, doi:10.1016/S0168-9002(03)00329-2.

[49] A. Valassi and R. Chierici, "Information and treatment of unknown correlations in the combination of measurements using the BLUE method", *Eur. Phys. J.* **C74** (2014) 2717, doi:10.1140/epjc/s10052-014-2717-6, arXiv:1307.4003.

[50] G. Corcella et al., "HERWIG 6.5: An event generator for hadron emission reaction with interfering gluons", *JHEP* **01** (2001) 010, arXiv:0011363.

[51] S. Frixione and B. Webber, "Matching NLO QCD computations and parton shower simulations", *JHEP* **0206** (2002) 029, arXiv:0204244.

[52] A. Buckley et al., "Rivet user manual", *Comput. Phys. Commun.* **184** (2013) 2803–2819, doi:10.1016/j.cpc.2013.05.021, arXiv:1003.0694.

[53] M. Dobbs and J. B. Hansen, "The HepMC C++ Monte Carlo event record for High Energy Physics", *Comput. Phys. Commun.* **134** (2001) 41–46, doi:10.1016/S0010-4655(00)00189-2.

[54] J. Alwall et al., "The automated computation of tree-level and next-to-leading order differential cross sections, and their matching to parton shower simulations", *JHEP* **1407** (2014) 079, doi:10.1007/JHEP07(2014)079, arXiv:1405.0301.

[55] T. Gleisberg et al., "Event generation with SHERPA 1.1", *JHEP* **0902** (2009) 007, doi:10.1088/1126-6708/2009/02/007, arXiv:0811.4622.

[56] T. Sjöstrand, S. Mrenna, and P. Z. Skands, "A Brief Introduction to PYTHIA 8.1", *Comput. Phys. Commun.* **178** (2008) 852–867, doi:10.1016/j.cpc.2008.01.036, arXiv:0710.3820.

[57] M. Botje et al., "The PDF4LHC Working Group Interim Recommendations", arXiv:1101.0538.

[58] A. D. Martin, W. J. Stirling, R. S. Thorne, and G. Watt, "Uncertainties on α_s in global PDF analyses and implications for predicted hadronic cross sections", *Eur. Phys. J.* **C64** (2009) 653–680, doi:10.1140/epjc/s10052-009-1164-2, arXiv:0905.3531.

[59] J. Gao et al., "CT10 next-to-next-to-leading order global analysis of QCD", *Phys. Rev.* **D89** (2014), no. 3, 033009, doi:10.1103/PhysRevD.89.033009, arXiv:1302.6246.

[60] R. D. Ball et al., "Parton distributions with LHC data", *Nuclear Physics B* **867** (2013), no. 2, 244 – 289, doi:http://dx.doi.org/10.1016/j.nuclphysb.2012.10.003.